frontiers in Bioengineering and Biotechnology

ORIGINAL RESEARCH
published: 14 July 2020
doi: 10.3389/fbioe.2020.00783

# Ultrasound Molecular Imaging as a Potential Non-invasive Diagnosis to Detect the Margin of Hepatocarcinoma via CSF-1R Targeting

*Qiongchao Jiang[1,2†], Yunting Zeng[1,2†], Yanni Xu[1,2†], Xiaoyun Xiao[1†], Hejun Liu[3], Boyang Zhou[1,2], Yao Kong[1,2], Phei Er Saw[4]* and Baoming Luo[1]**

[1] Department of Ultrasound, Sun Yat-sen Memorial Hospital, Sun Yat-sen University, Guangzhou, China, [2] Guangdong Provincial Key Laboratory of Malignant Tumor Epigenetics and Gene Regulation, Sun Yat-sen Memorial Hospital, Sun Yat-sen University, Guangzhou, China, [3] Department of Hyperbaric Oxygen, Sun Yat-sen Memorial Hospital, Sun Yat-sen University, Guangzhou, China, [4] Guangdong Provincial Key Laboratory of Malignant Tumor Epigenetics and Gene Regulation, Medical Research Center, Sun Yat-sen Memorial Hospital, Sun Yat-sen University, Guangzhou, China

Though radiofrequency ablation (RFA) is considered to be an effective treatment for hepatocellular carcinoma (HCC), but more than 30% of patients may suffer insufficient RFA (IRFA), which can promote more aggressive of the residual tumor. One possible method to counter this is to accurately identify the margin of the HCC. Colony-stimulating factor 1 receptor (CSF-1R) has been found to be restrictively expressed by tumor associated macrophages (TAMs) and monocytes which more prefer to locate at the boundary of HCC. Using biotinylation method, we developed a CSF-1R-conjugated nanobubble CSF-1R ($NB_{CSF-1R}$) using a thin-film hydration method for margin detection of HCC. CSF-1R expression was higher in macrophages than in HCC cell lines. Furthermore, immunofluorescence showed that CSF-1R were largely located in the margin of xenograft tumor and IFRA models. *In vitro*, $NB_{CSF-1R}$ was stable and provided a clear ultrasound image even after being stored for 6 months. In co-culture, $NB_{CSF-1R}$ adhered to macrophages significantly better than HCC cells ($p = 0.05$). In *in vivo* contrast-enhanced ultrasound imaging, the washout half-time of the $NB_{CSF-1R}$ was significantly greater than that of $NB_{CTRL}$ and Sonovue® ($p = 0.05$). The signal intensity of the tumor periphery was higher than the tumor center or non-tumor region after $NB_{CSF-1R}$ injection. Taken together, $NB_{CSF-1R}$ may potentially be used as a non-invasive diagnostic modality in the margin detection of HCC, thereby improving the efficiency of RFA. This platform may also serve as a complement method to detect residual HCC after RFA; and may also be used for targeted delivery of therapeutic drugs or genes.

**Keywords: ultrasound imaging, HCC tumor margin, non-invasive tumor margin detection, CSF-1R targeting, macrophage**

OPEN ACCESS

***Edited by:***
*Jianxun Ding,*
*Changchun Institute of Applied Chemistry (CAS), China*

***Reviewed by:***
*Wenjun Miao,*
*Nanjing Tech University, China*
*Qingqing Xiong,*
*Tianjin Medical University Cancer Institute and Hospital, China*
*Wenliang Li,*
*Jilin Medical University, China*

****Correspondence:***
*Phei Er Saw*
*caipeie@mail.sysu.edu.cn*
*Baoming Luo*
*luobm@mail.sysu.edu.cn*

*† These authors have contributed equally to this work*

***Specialty section:***
*This article was submitted to Biomaterials, a section of the journal Frontiers in Bioengineering and Biotechnology*

***Received:*** *10 May 2020*
***Accepted:*** *22 June 2020*
***Published:*** *14 July 2020*

***Citation:***
*Jiang Q, Zeng Y, Xu Y, Xiao X, Liu H, Zhou B, Kong Y, Saw PE and Luo B (2020) Ultrasound Molecular Imaging as a Potential Non-invasive Diagnosis to Detect the Margin of Hepatocarcinoma via CSF-1R Targeting. Front. Bioeng. Biotechnol. 8:783. doi: 10.3389/fbioe.2020.00783*

## INTRODUCTION

Hepatocellular carcinoma (HCC), is the third leading cause of cancer death in China (Chen et al., 2016). Radiofrequency ablation (RFA) which considered to be a valid local treatment method with curative intent and shows a comparable overall outcome to that of liver resection when patients with HCCs smaller than 3 cm in diameter (N'Kontchou et al., 2009; Kang et al., 2015). However, one major cause of insufficient RFA (IRFA) is the uncertain ablation margin, which may lead to local recurrence with a more aggressive phenotype and worse prognosis (Kim et al., 2010; Wang et al., 2013; Liu et al., 2015; Shady et al., 2016; Sotirchos et al., 2016; Dai et al., 2017; Zhang et al., 2019).

Some researchers found that colony-stimulating factor 1 receptor (CSF-1R) expression and tumor associated macrophage (TAM) density (CSF-1 receptor, CSF-1R or CD68) in the adjacent liver tissues are associated with patient survival after resection of HCC (Zhu et al., 2008; Jia et al., 2010; Kong et al., 2013). CSF-1R is highly expressed by monocytes (precursors of macrophages) and TAMs which support tumor cell proliferation, motility, and drug resistance (Lewis and Pollard, 2006; Pyonteck et al., 2013). CSF-1R and macrophages are the front line of defense to prevent tumor growth. The peritumoral liver tissue, which possessed of abundant CSF-1R, plays an opposite role in anti-tumor effect by providing a fertile environment for metastasis (Qian and Pollard, 2010). A high density of CSF-1R in peritumoral liver tissue, but not in tumor tissue, was associated with poor survival and a high incidence of metastasis after resection of the primary tumor (Zhu et al., 2008; Nandi et al., 2013). Leftin et al., 2019 confirmed that macrophage-targeted inhibition of CSF-1R by immunotherapy inhibits macrophage accumulation and slows mammary tumor growth *in vivo*. Thus, CSF-1R might be a feasible target for molecular imaging of HCC.

Ultrasound molecular imaging can provide high specificity and sensitivity imaging as it combines the advantages of ultrasound contrast agents (UCAs). UCAs can targeted with ligands such as antibodies or other proteins to detect expression of cancer-specific molecular markers (Jiang et al., 2016; Li et al., 2018; Wang et al., 2018). Unfortunately, traditional UCAs composed of microbubbles with a diameter about several micrometers, which cannot penetrate through the vasculature and have the short circulation time, which has constrained the advancement of ultrasound molecular imaging (Krupka et al., 2010; Wang et al., 2010). Nanobubbles (NBs, <1000 nm) were then introduced as a contrast agent enhancer in ultrasound imaging. However, NBs may decrease the echogenicity under clinical ultrasound (Sheeran et al., 2013). So it extremely challenging to fabricate not only small, highly echogenic particles but also can provide new, paradigm shifting applications of ultrasound agents in diagnosis and therapy (theranostics; Guvener et al., 2017; Tang et al., 2017; Liu et al., 2019).

Herein, to address the above shortcomings, we designed a novel CSF-1R targeted nanobubble ($NB_{CSF-1R}$) and characterized its properties *in vitro* and *in vivo*. We also investigated the specificity and efficacy of the nanobubbles ($NB_{CTRL}$ and $NB_{CSF-1R}$) against HCC xenograft tumors and IRFA models to evaluate the feasibility of using $NB_{CSF-1R}$ in the clinical diagnosis of HCC margin (**Scheme 1**).

## MATERIALS AND METHODS

### Materials

1,2-distearoyl-sn-glycero-3-phosphocholine (DSPC) and 1,2-dipalmitoyl-sn-glycero- 3-phosphoethanolamine (DPPE) were purchased from Avanti Polar Lipids, Inc. (Alabaster, AL, United States). Polyethylene glycol (PEG4000) was

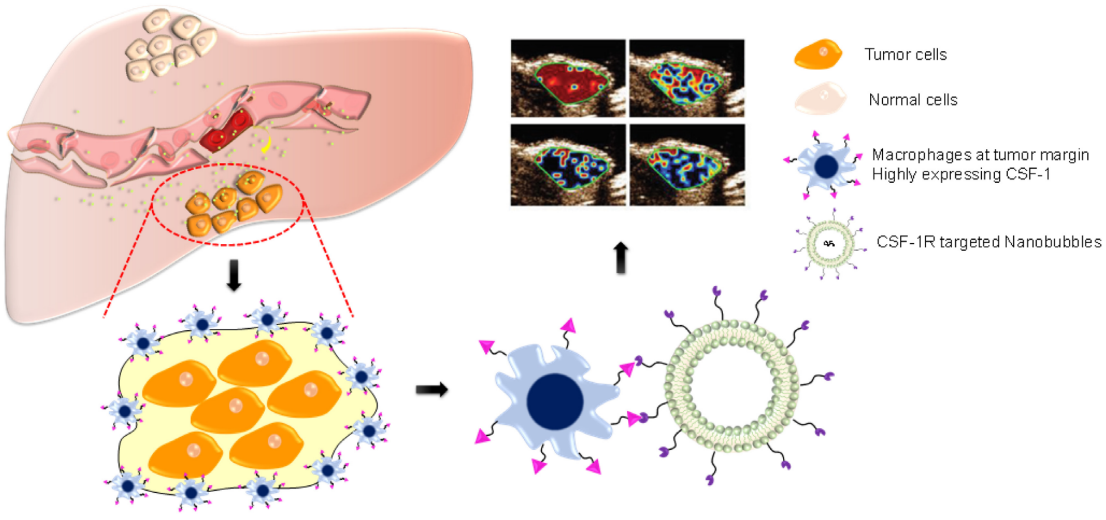


**SCHEME 1 |** After radiofrequency ablation (RFA), macrophages are highly condensed at the tumor margin, highly expressing CSF-1R. By using nanobubbles targeting CSF-1R ($NB_{CSF1R}$), we developed an ultrasound-guided CSF-1R specific targeted real-time monitoring of tumor margin. $NB_{CSF1R}$ could penetrate through the vascular and adhered to the macrophages, which can provide ultrasound molecular imaging to reveal the accurate margin of HCC.

purchased from Aladdin Limited Company (Shanghai, China). 1,2-distearoyl-sn-glycero-3-phosphoethanolamine-N-[biotinyl(polyethylene glycol)-2000] (DSPE-$PEG_{2000}$-Biotin) was purchased from A.V.T. Pharmaceutical Co., Ltd. (Shanghai, China). 4′,6-diamidino-2-phenylindole (DAPI) and 1,1′-dioctadecyl-3,3,3′,3′-tetramethylindocarbocyanineperchlorate (DiI) were obtained from Beyotime (Haimen, China). Octafluoropropane ($C_3F_8$) was purchased from Guangzhou Walter (Guangzhou, China). Antibodies for flow cytometric analysis or Western blot of CSF-1R were purchased from Novus International, Inc. (St Charles, MO, United States). Antibodies for immunohistochemistry (IHC) or immunofluorescence (IF) for CSF-1R were obtained from Abcam (Cambridge, MA, United States). Other chemicals and reagents were of analytical grade. Phorbol 12-myristate 13-acetate (PMA) was purchased from Sigma-Aldrich (St. Louis, MO, United States).

## Cells

Human monocyte THP-1 was purchased from Sun Yat-sen University Cell Bank. SMMC-7721 and HepG2 human liver cancer cell lines were kindly donated by the Radiology Department, Sun Yat-sen Memorial Hospital. The H22 cell line was obtained from Procell Life Science & Technology Co., Ltd. (Wuhan, China). Hepa1-6 mouse liver cancer cell lines were purchased from Guangzhou Genebio Biotechnology Co., Ltd. (Guangzhou, China). SMMC-7721, HepG2, and Hepa1-6 cells were cultured in Dulbecco's modified Eagle's medium (DMEM, GIBCO Gaithersburg, MD, United States) and supplemented with high glucose and 10% fetal bovine serum (FBS, GIBCO) at 37°C with 5% $CO_2$. THP-1 and H22 were cultured separately in RPMI 1640 (GIBCO) and supplemented with 10% FBS at 37°C with 5% CO2. Macrophages were obtained from induction of THP-1 cells by 100 ng/ml of PMA for 24 h.

## Animals

All animal procedures were performed in accordance with the Guidelines for Care and Use of Laboratory Animals of Sun Yat-sen University. Experiments were reviewed and approved (NO. SYSU-IACUC-2018-000179) by the Ethics Committee of Sun Yat-sen Memorial Hospital and Ethics Committee of Zhongshan School of Medicine (ZSSOM) on Laboratory Animal Care, Sun Yat-sen University (Guangdong, China).

## Patients and Tissue Samples

Primary hepatocellular carcinomas were obtained from 30 patients at Sun Yat-sen Memorial Hospital. All samples were collected with informed consent and with the approval of the Internal Review and Ethics Boards of the indicated hospitals.

## Expression of CSF-1R *in vitro*

Quantitative real-time polymerase chain reaction (qRT-PCR), fluorescence-activated cell sorting (FACS), and Western blot were used to analyze the CSF-1R presentation in different cells. The following primers were used: human CSF-1R: forward (5′- > 3′) AGCGATAGGTCCCCGTGTTTT, reverse (5′- > 3′) CAACGGTGACCTTGCGATGTG, murine CSF-1R: forward (5′- > 3′) CAGGGTCCAAGGTCCAGTAGG, reverse (5′- > 3′) TGGTTGTAGAGCCGGGTGAAA. Macrophages and SMMC-7721 cells were seeded into six-well plates at $5 \times 10^5$ cells/well in 2 mL of medium for 12 h. Cells were collected and each sample was divided into two tubes. One tube was incubated with anti-CSF-1R antibodies for 30 min and then rinsed with phosphate-buffered saline (PBS) one time. Then, the samples were incubated with PE-conjugated anti-mouse IgG for 20 min and rinsed with PBS. The fluorescence intensity in the macrophages and SMMC-7721 cells was calculated by Flow Cytometry (Beckman Coulter, Fullerton, CA, United States).

## Expression of CSF-1 *in vivo*

Immunohistochemistry (IHC) analysis of human liver cancer tissue and peritumor tissue adjacent to tumor (about 10 mm) was performed. Procedures for IHC analysis of CSF-1R (anti-CSF-1R antibody, 1:200 dilution, Novus International, Inc., United States) were performed. Procedures for IHC analysis of CSF-1R (anti-CSF-1R antibody, ab215441, 1:100 dilution, Abcam, Cambridge, MA, United States) were performed in two random fields in tumor tissue and peritumor tissue for each slide. The quantification of stained cells was analyzed by Image-Pro Plus. The slides were observed by using a light microscope (ECLIPSE 80i, Nikon, Japan).

## Preparation of the Nanobubbles

Nanobubbles were prepared according to our previous studies (Jiang et al., 2016; Zhou et al., 2019). Briefly, a homogenous mixture containing DSPE-$PEG_{2000}$-biotin, DSPE-$PEG_{2000}$, DSPC, and DPPE at a mole ratio of 2.5:2.5:30:10 was mixed in 15 mL chloroform. The mixture was stirred for 1 h, then vacuum dried for 2 h at 60°C using a rotary evaporator (EYELA, Tokyo, Japan). The resulting film was rehydrated with PBS and agitated for 2 h. The size of the resulting liposomes was reduced by sonication, and then $C_3F_8$ gas was injected to replace the air over the fluid to generate NBs.

The bubbles were purified by centrifugation and collected according to our previous research. Then, NBs were resuspended in PBS and stored at 4°C. For the development of fluorescent NBs, DiI-encapsulated NBs were prepared through the same method, with the addition of DiI in the initial mixture of phospholipids in chloroform. DiI-encapsulated $NB_{CSF-1R}$ were observed by inverted fluorescence microscope (Olympus IX73, Japan) and Western Blot. Excitation wavelength of Dil is 549 nm and the emission wavelength is 565 nm.

## Western Blot Analysis

In order to determine the success of CSF-1R onto NBs surface, SDS-PAGE and Western blot were used. An 8% SDS–polyacrylamide gel was loaded with $NB_{CTRL}$, $NB_{CSF-1R}$, and $CSF\text{-}1R_{mAb}$ (Novus International, Inc., United States) and electrophoresed under reducing condition for 2 h at 60 mV and for an additional 180 min at 300 mA. The gel was then transferred to a membrane and blocked using 5% skim milk. After blocking, the membranes were Horseradish peroxidase (HRP)-conjugated goat anti-rabbit IgG (1:2000 dilution; Santa

Cruz Biotechnology, Santa Cruz, CA, United States) was used as the secondary antibody. Protein signals were detected using a chemiluminescence system (New Life Science Products, Boston, MA, United States).

## Preparation of $NB_{CSF-1R}$

*In vitro* CSF-$1R_{mAbs}$ was biotinylated using the EZLink NHS-Biotin Kit (Muralidhara et al., 2019; Wang et al., 2019). Biotinylated CSF-$1R_{mAb}$ was bound to the NBs ($NB_{CTRL}$) by linking the biotin groups of CSF-$1R_{mAb}$ and DSPE-$PEG_{2000}$-biotin on the NBs with Streptavidin. Briefly, nanobubbles was mixed with biotinylated CSF-$1R_{mAb}$ using a DSPE-$PEG_{2000}$-biotin:CSF-$1R_{mAb}$: Streptavidin molar ratio of 30:1:15, then incubated at 4°C for 8 h ($NB_{CSF-1R}$). To remove the excess free CSF-$1R_{mAb}$, the upper layer of the suspension was centrifuged three times (1000 rpm, 5 min) and stored at 4°C. To determine the success of conjugation, the CSF-$1R_{mAb}$ was labeled with fluorescein isothiocyanate (FITC) and co-localization of the CSF-$1R_{mAb}$ with CSF-1R were confirmed by fluorescence microscope.

## Characterization of $NB_{CTRL}$ and $NB_{CSF-1R}$

### Size, Zeta, Concentration, TEM, and Stability Test

The mean diameter and Zeta potential of $NB_{CTRL}$, and $NB_{CSF-1R}$ were measured using a Malvern Zetasizer Nano (Malvern Instruments, Ltd., United Kingdom). Their morphology was detected by scanning electron microscopy (SEM, SU8020, Hitachi, Japan). The concentration of NBs was measured with a Coulter counter (Multisizer 4e, United States) according to Liu et al. (2019).

The long-term stability test of $NB_{CSF-1R}$ were confirmed by using a Vevo 2100 small animal imaging device with a frequency of 20 MHz, in a static state. $NB_{CSF-1R}$ was diluted from 100 to 10,000 times. The contrast imaging was then observed for each sample. To determine the long-term stability of $NB_{CSF-1R}$, the above experiments were repeated in samples that had been stored for 1, 3, or 6 months at 4°C. As a control, Sonovue® was suspended at the same concentration.

## Cytotoxicity Analysis

Macrophages were induced from THP-1 cells. Approximately $5 \times 10^6$ cells were cultured with 100 ng/ml PMA for 24 h at 37°C with 5% $CO_2$. SMMC-7721 cells and macrophages were separately inoculated into 96-well plates at 3000 cells/well for 12 h. The same volume of fresh media with various concentrations $NB_{CSF-1R}$ were incubated with the cells for an additional 24 h, the concentration of $NB_{CSF-1R}$ ranging from $2 \times 10^3$ to $2 \times 10^8$ bubbles/ml. Then, 10 μL CCK-8 reagent in 100 μL fresh medium replaced, and incubated for an additional 2 h. The plates were gently shook for 5 min, and Infinite F200 multimode plate reader (Spectra Max M5, Molecular Devices) was used to test the absorbance of each well at 450 nm. All experiments were conducted in triplicate.

## *In vitro* Targeting Ability of $NB_{CSF-1R}$

SMMC-7721 and macrophages were seeded into confocal dishes at $1 \times 10^5$ cells/dish and grown for 24 h at 37°C with 5% $CO_2$. The cells were then rinsed gently with PBS three times at room temperature, 4% paraformaldehyde was added for 5 min, then cells were gently rinsed again with PBS three times. Then, 1 ml of PBS containing 0.5% Triton X-100 was added for 5 min and rinsed with PBS three times. The remaining steps were performed in the dark: added 100 μL of diluted phalloidin solution (5 μL of phalloidin solution to 200 μL of PBS containing 0.1% BSA) to cover the cells in the center of the confocal dish; incubated for 30 min; added 200 μL DiI labeled $NB_{CSF-1R}$ or $NB_{CTRL}$ to the center of the confocal dish and incubated for 2 h at 37°C with 5% $CO_2$; added 200 μl of 100 ng/ml DAPI solution and incubated for 5 min; gently rinsed 5 times with PBS to remove the unbound CSF-1R. The cells were observed under a laser confocal microscope to observe the fluorescence distribution of the cytoskeleton and the $NB_{CSF-1R}$, and the specific targeting of the $NB_{CSF-1R}$ to the CSF-1 was observed.

## *In vivo* Contrast-Enhanced Imaging

To generate tumors, approximately $1 \times 10^7$ SMMC-7721 cells in 100 μL of single-cell suspension was injected into 5–6-week-old male BALB/c nude mice ($n = 30$, five animals/group) in the right hind legs, subcutaneously (*s.c.*). The mean maximum tumor size at ultrasound was about 10 mm. In this experiment, the mice were divided into six groups ($n = 30$). Group 1 = $NB_{CTRL}$, Group 2 = $NB_{CSF-1R}$, Group 3 = Sonovue, Group 4 = $NB_{CTRL}$ + IRFA, Group 5 = $NB_{CSF-1R}$ + IRFA, Group 6 = Sonovue® + IRFA. During imaging, Mice were kept warm using a heated stage and a heat lamp, and anesthesia at 2% isoflurane in oxygen at 2 L/min during imaging. Mechanically, the contrast enhanced imaging can only generated while enveloped bubbles undergo compression and expansion. In this experiment, negative blank (PBS) was not included as PBS was unable to generate ultrasound intensity. Three groups received radiofrequency ablation to simulate IRFA models, which was performed using a bipolar RFA device (Radionics, INC, Burlington, MA, United States), radiofrequency energy about 30 watts for 30 s. One group of the xenograft tumor models and one group of the residual cancer models received $NB_{CSF-1R}$. Mice were anesthetized with isoflurane by full anesthesia machine and placed on a warm pad. Approximately, $4 \times 10^7$ $NB_{CSF-1R}$ was injected through caudal veins. The ultrasound contrast parameters were: (Visual Sonics, Vevo 2100) Transducer: MS-250; Frequency: 20 MHz; Imaging Mode: Non-linear Contrast Mode; Dynamic Range: 30 dB; Overall Contrast Gain: 45 dB; Output Power: 4%. $NB_{CTRL}$ and Sonovue® were injected through caudal veins similarly. VevoCQ software was used to export the image of ultrasound molecular imaging (USMI) signal, and then observe the differential targeted enhancement distribution in the region of interest (green contour).

## Statistical Analysis

For data analysis, Statistical Package for the Social Sciences (SPSS) version-21 (SPSS, Inc., Chicago, IL, United States) was

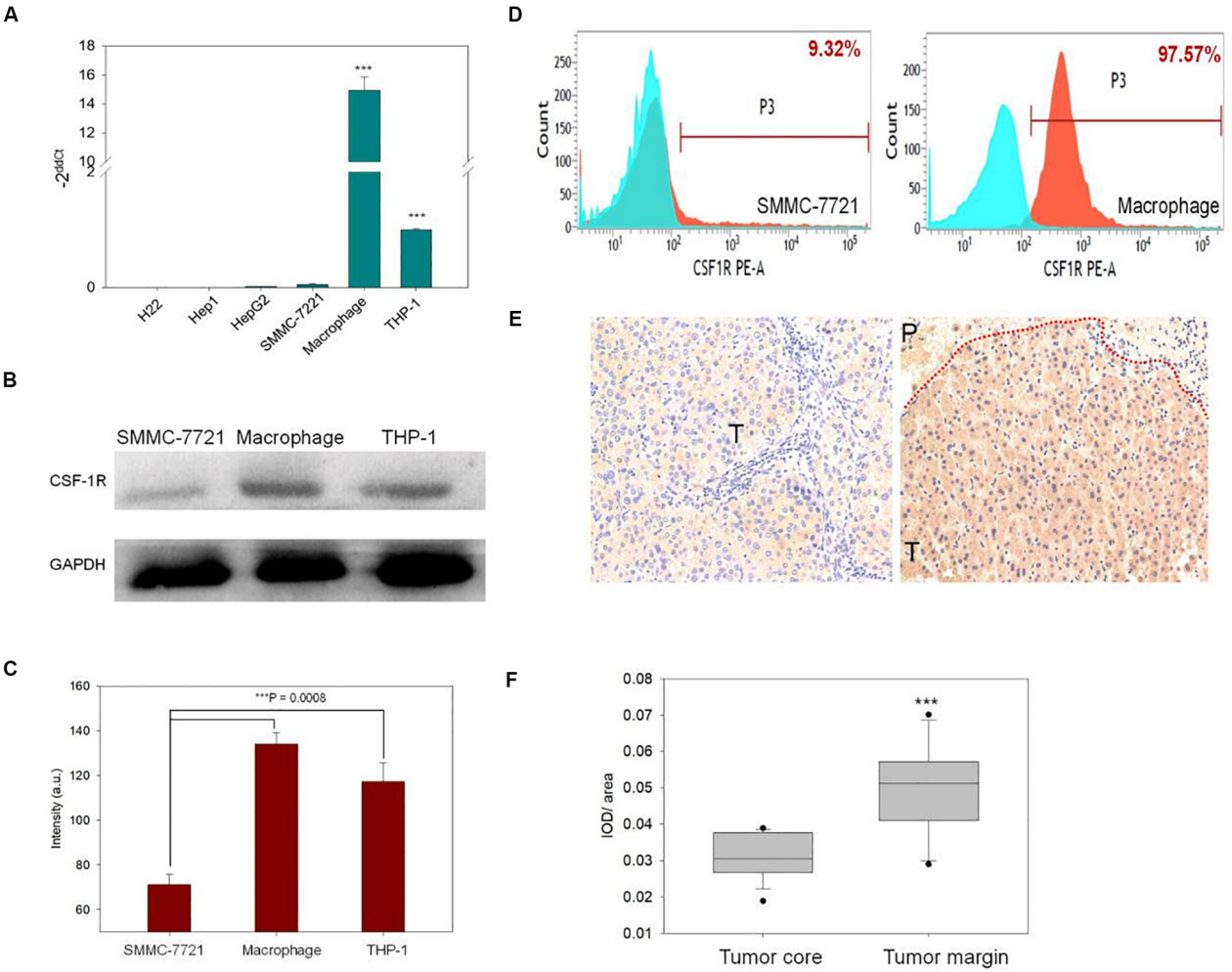


**FIGURE 1 | (A)** qRT-PCR was used to determine the expression of colony-stimulating factor 1 receptor (CSF-1R) in different cell lines. **(B)** Western blot was used to access the protein level of CSF-1R in macrophages, THP-1, and SMMC-7721. **(C)** Showed the CSF-1R expression intensity in macrophages, THP-1, and SMMC-7721, macrophages showed the highest intensity than THP-1 and SMMC-7721, (***indicates $p < 0.01$). **(D)** The expression level of CSF-1R in macrophages and SMMC-7721 were detected by fluorescence-activated cell sorting (FACS) blue indicated the control group and, red indiacted the experiment group. **(E)** IHC verified the expression distribution of CSF-1R in human liver cancer tissues (the red line indicated the boundary of hepatocellular carcinoma (HCC). (P, peritumoral, T, tumor). **(F)** Semi-quantitatively analyzed the expression of CSF-1R by image-pro plus (IPP) software (***indicates $p < 0.01$).

used. GraphPad Prism version 5.00 (GraphPad Software, Inc., San Diego, CA, United States) was used to generate figures. $p < 0.05$ was considered statistically significant. Data from the experiments was expressed as mean ± SD for technical replicates and the mean ± SEM for biological replicates. ANOVA was performed to compare differences between multiple groups and Differences in continuous variables were analyzed by Student's *t*-test to compare two groups. A non-parametric test of two paired samples was analyzed by Wilcoxon Signed Rank Test.

# RESULTS

## CSF-1R Expression *in vitro* and *in vivo*

To verify the expression of CSF-1R *in vitro*, qRT-PCR, Flow Cytometry, and Western blot were carried out. As seen in **Figure 1A**, qRT-PCR analysis revealed that the expression of CSF-1R mRNA is significantly higher in macrophages as compared to H22, SMMC-7721, HepG2, Hepa1-6, and THP-1 ($p = 0.05$). We then proceed to select a mouse originated cell line SMMC-7721 for consideration of *in vivo* experiments. Western blot analysis also confirmed that the protein level of CSF-1R is overexpressed in macrophages and THP-1, while minimally expressed in SMMC-7721 cells (**Figure 1B**). Comparison of CSF-1R intensity showed a significantly greater extent of expression within macrophages (macrophage: intensity of 143.75 ± 4.2 a.u.; THP-1: 103.02 ± 3.4 a.u.; SMMC-7721: 78.36 ± 3.4 a.u.; $p < 0.001$; **Figure 1C**). Quantification analysis using FACS indicated that 97.57% of macrophages are CSF-1R positive compared to 9.32% of SMMC-7721 cells (**Figure 1D**).

Immunohistochemistry analysis was carried out to confirm the expression of CSF-1R in HCC patients. As seen in **Figure 1E**, CSF-1R deposits were detected in the peritumoral tissues of carcinoma *in situ* in human HCC (**Figure 1E**). The counts of

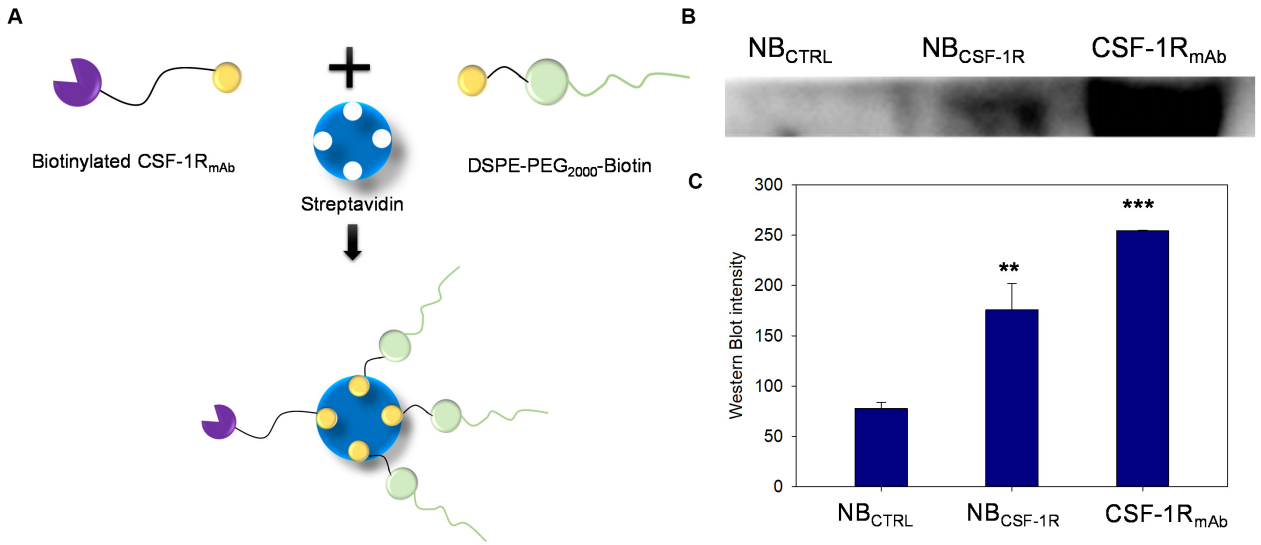


**FIGURE 2 | (A)** The process of synthesis of nanobubble CSF-1R ($NB_{CSF-1R}$) through the streptavidin/biotin chemical effect, CSF-$1R_{mAb}$ was biotinylated and then conjunction to the 1,2-distearoyl-sn-glycero-3-phosphoethanolamine-N-[biotinyl(polyethylene glycol)-2000] (DSPE-$PEG_{2000}$)-Biotin. **(B)** Western blot showed that the $NB_{CSF-1R}$ band was at approximately the same position as CSF-$1R_{mAb}$, and the $NB_{CTRL}$ showed no expression of CSF-1R. **(C)** Showed the Western blot intensity of $NB_{CSF-1R}$, CSF-$1R_{mAb}$, $NB_{CTRL}$ (**indicates $p < 0.05$, ***indicates $p < 0.001$).

positive CSF-1R differed significantly between the normal tissue and the margin ($p < 0.05$; **Figure 1F**).

## NPs Synthesis and Characterization Particle Surface Modification

**Figure 2A** shows the schematic illustration of $NB_{CSF-1R}$ fabrication through Streptavidin/biotin interaction. Western blot showed that the band intensity of CSF-1R attached on $NB_{CSF-1R}$ was similar with CSF-1R input, while $NB_{CTRL}$ showed no indication of CSF-1R band (**Figure 2B**), indicating that CSF-1R successfully conjugated with the $NB_{CSF-1R}$ specifically ($p < 0.005$; **Figure 2C**).

**Figure 3A** depicted the two NBs synthesized, the non-targeted $NB_{CTRL}$ and the targeted $NB_{CSF-1R}$. The morphologies of $NB_{CTRL}$ and $NB_{CSF-1R}$ were observed by SEM. As shown in **Figures 3B,C**, $NB_{CTRL}$ and $NB_{CSF-1R}$ were spherical, uniformed in size and had distinct shell structures. The physical properties of $NB_{CTRL}$ and $NB_{CSF-1R}$ are summarized in **Figure 3D**. Dynamic laser scattering (DLS) analysis indicated that the average hydrodynamic size of $NB_{CTRL}$ and $NB_{CSF-1R}$ was (408.0 ± 17.5) nm and (428.0 ± 12.47) nm, respectively. Zeta potential values showed that $NB_{CTRL}$ was with charge of −4.03 ± 0.23 mV, and $NB_{CSF-1R}$ was −4.42 ± 0.51 mV. The concentrations of $NB_{CTRL}$ and $NB_{CSF-1R}$ were (5.99 ± 0.08) × $10^8$ bubbles/mL ($n = 5$) and (4.24 ± 0.07) × $10^8$ bubbles/mL ($n = 5$), respectively.

## CSF-1R-Binding Efficiency to the NBs

To illustrate the *in vitro* binding efficacy and co-localization of $NB_{CSF-1R}$ with CSF-1R, we synthesized DiI-labeled $NB_{CTRL}$ while CSF-$1R_{mAb}$ were labeled with FITC. After co-incubation, the cells were observed under microscope. The green light of the FITC-labeled antibody (**Figure 4A**) and the red light of the DiI-labeled nanobubbles (**Figure 4B**) merged perfectly (**Figure 4C**), indicating that CSF-$1R_{mAb}$ were successfully attached to the NBs, and could specifically target CSF-1R.

## *In vitro* Cytotoxicity and Stability of $NB_{CTRL}$ and $NB_{CSF-1R}$

After the induction of THP-1 cells into macrophages by 100 ng/ml PMA, the cells changed from suspension state to adherent state, and some of the cells became spindle-like, which confirmed that successful induction of THP-1 cells into macrophages. The cytotoxicity of $NB_{CTRL}$ and $NB_{CSF-1R}$ was evaluated using SMMC-7721 and macrophages incubated with $NB_{CTRL}$ at five concentrations between $10^8$ and $10^3$/mL for 24 h (**Figure 5A**). Both SMMC-7721 and macrophages incubated with $NB_{CTRL}$ did not show significant changes in cell viability in all concentration after 24 h of incubation. The cell viability of both SMMC-7721 cells and macrophages remained (85% after incubation with either type of $NB_{CTRL}$, indicating they were minimally cytotoxic. These results show that $NB_{CTRL}$ and $NB_{CSF-1R}$ have good biocompatibility and cause minimal harm to the tested cells.

The echogenic properties of $NB_{CSF-1R}$ were investigated in agarose gel phantom in comparison to Sonovue® *in vitro*, using a Vevo 2100 small animal imaging device with a frequency of 20 MHz. The signal enhancements of $NB_{CSF-1R}$ stored at 4°C for different periods of time (0, 30, 90, 120, and 180 days) were investigated. As indicated in **Figure 5B**, echogram result of NBs at Day-180 indicated no significant difference between NBs and Sonovue® at Day-0 indicating that the $NB_{CSF-1R}$ was stable.

The capability of $NB_{CSF-1R}$ was also assessed *in vitro* using a Vevo 2100 small animal imaging device with a frequency of 20 MHz at various concentrations. Different concentrations of $NB_{CSF-1R}$ nanoparticles (approximately

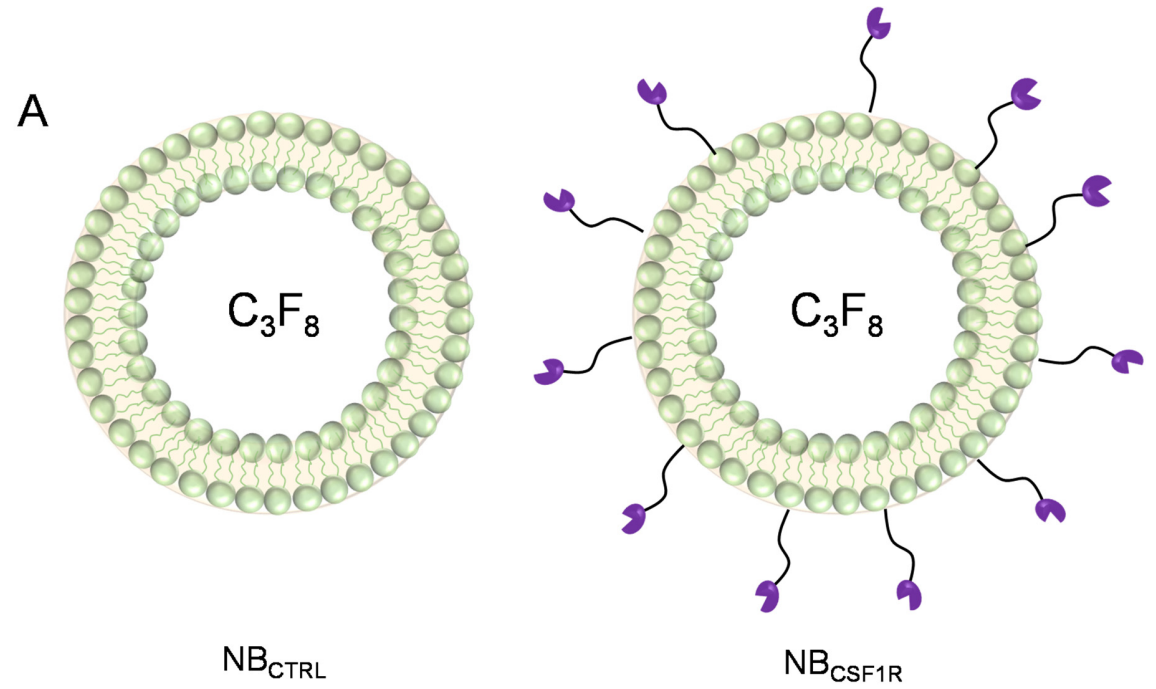


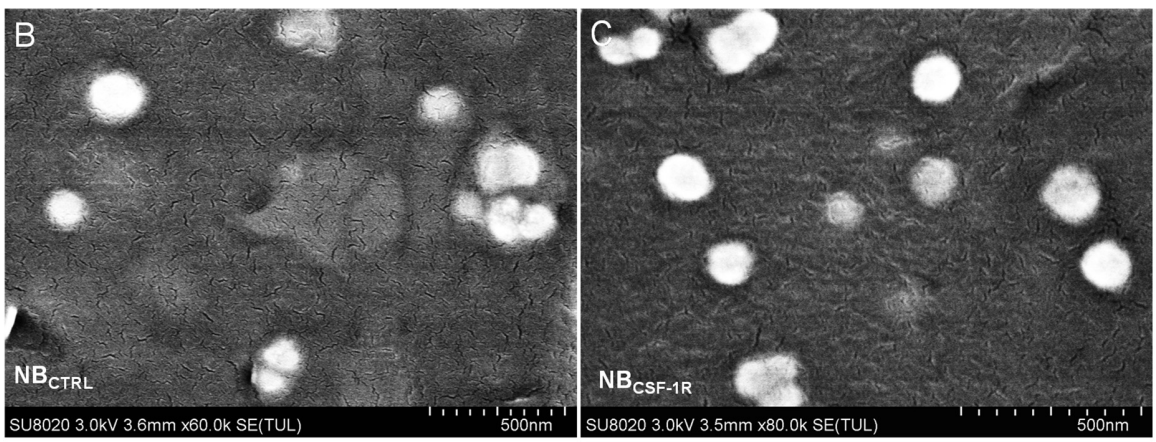


D

| | Size (nm) | Zeta potential (mV) | Concentration (x$10^8$ / mL) |
|---|---|---|---|
| $NB_{CTRL}$ | 408.0 ± 17.50 | -4.03 ± 0.23 | 5.99 ± 0.08 |
| $NB_{CSF-1R}$ | 428.0 ± 12.47 | -4.42 ± 0.51 | 4.24 ± 0.07 |

**FIGURE 3 | (A)** Showed the structure of the $NB_{CTRL}$ and $NB_{CSF-1R}$, **(B)** scanning electron microscopy (SEM) image of $NB_{CTRL}$ with a scale bar of 500 nm **(C)** SEM image of $NB_{CSF-1R}$ with a scale bar of 500 nm. **(D)** Summary of the average size, and zeta potential of $NB_{CTRL}$ and $NB_{CSF-1R}$ as measured by dynamic laser scattering. Concentration of NBs were measured by Coulter counter. Data represent mean ± SD ($n$ = 5).

$1 \times 10^4$ ~$6.0 \times 10^6$/bubbles of same volume, 100 μL) were evaluated in this experiment. The signal intensity decreased with the decreasing concentrations of $NB_{CSF-1R}$ (**Figure 6A**). However, even when the $NB_{CSF-1R}$ were diluted 2000 times, the signal intensity remained relatively strong.

To determine the binding ability of $NB_{CTRL}$ and $NB_{CSF-1R}$ in SMMC-7721 cells and macrophages, we carried out confocal laser scanning microscopy (CLSM) assay. The cytoskeletons with FITC phalloidin were green and the NBs labeled with DiI were red. As seen in **Figure 6B**, the red fluorescence intensity of macrophages

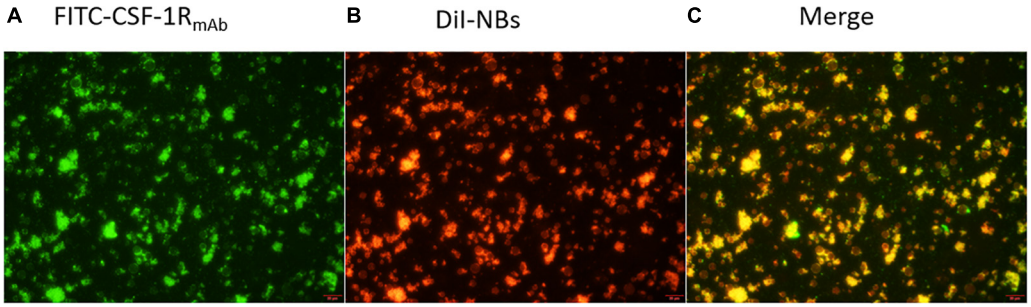


**FIGURE 4 |** Fluorescence microscopy image of target NBs. **(A)** CSF-1R$_{mAb}$ (FITC showed green fluorescence), **(B)** DiI-dyed (nanobubbles showed red fluorescence), and **(C)** their co-localization (merge) under fluorescence microscope, with a sale bar of 200 μm.

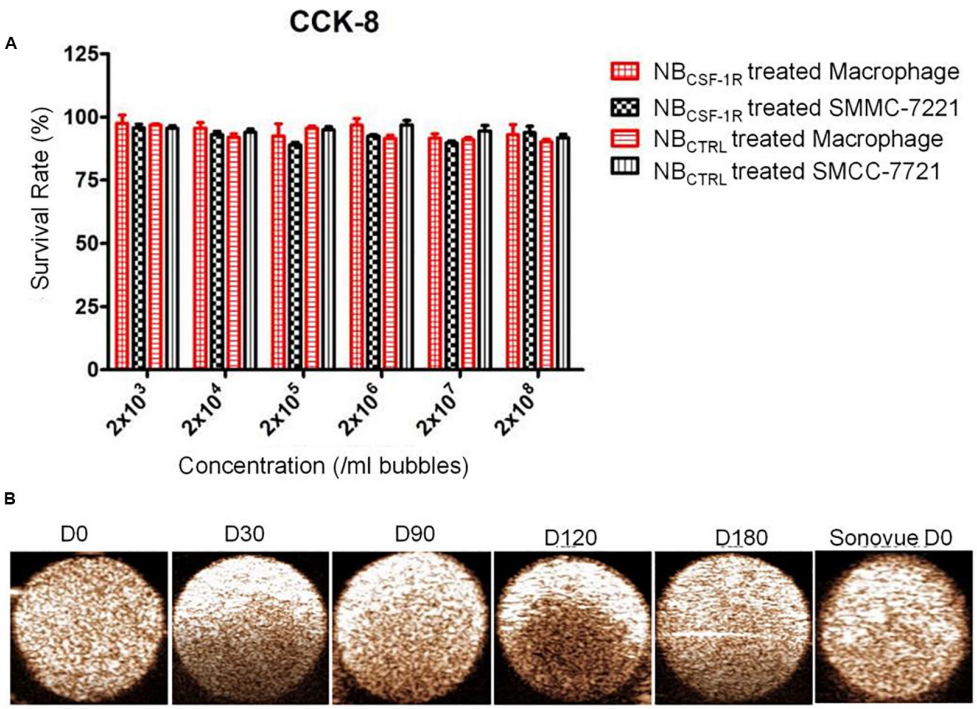


**FIGURE 5 | (A)** Cell viability test for NB$_{CSF-1R}$ determined through CCK-8. *In vitro* cytotoxicity assays using macrophage and (high CSF-1 expression) and SMMC-7721 cells (low CSF-1 expression) incubated with NB$_{CSF-1R}$ for 24 h; there was no significant difference in the viability of macrophages and SMMC-7721. **(B)** *In vitro* ultrasound images of NB$_{CSF-1R}$ stored for 0, 30, 90, 120, 180 days, and the Sonovue® stored for 0 days as a control. Ultrasound frequency, 20 MHz.

treated with NB$_{CSF-1R}$ was much higher than SMMC-7721 cells treated with NB$_{CSF-1R}$, NB$_{CTRL}$ and macrophages treated with NB$_{CTRL}$, while minimal attachment of NB$_{CSF-1R}$ and NB$_{CTRL}$ were seen in SMMC-7721. This result indicates that more NB$_{CSF-1R}$ adhered to macrophages, and demonstrated its excellent targeting ability.

## Stability and Ultrasound Sensitivity of the Targeted NBs *in vivo*

*In vivo,* NB$_{CSF-1R}$, NB$_{CTRL}$, and Sonovue® were tested in xenograft tumors and IRFA models which had been inoculated with SMMC-7721 cells ($n$ = 30, 5 mice for each group). After examination, none of the mice exhibited apparent signs of distress in each group, under the same ultrasound conditions. Contrast-enhanced images of the tumors continuously exposed to ultrasound were taken at minutes 0, 5, 15, and 30 (**Figures 7A,B**). The peak intensity and washout half-time were compared between NB$_{CSF-1R}$, NB$_{CTRL}$, and Sonovue® in these models (**Figures 7C,D**). The peak intensity of NB$_{CS-F1R}$, NB$_{CTRL}$, and Sonovue® (**Figure 7C**) was 11.55 ± 1.397 a.u, 8.826 ± 1.348 a.u, 12.20 ± 1.974 a.u in the xenograft tumors, and 12.67 ± 3.126 a.u, 13.74 ± 2.878 a.u, 11.53 ± 4.401 a.u in the IRFA models (**Figure 7C**). There was no significant difference between the groups (**Figures 7A,B**). The washout half-time of NB$_{CSF-1R}$, NB$_{CTRL}$, and Sonovue® in the xenograft tumors was 29.17 ± 1.08 min, 15.87 ± 1.05 min, 3.35 ± 0.16 min (**Figure 7D**),

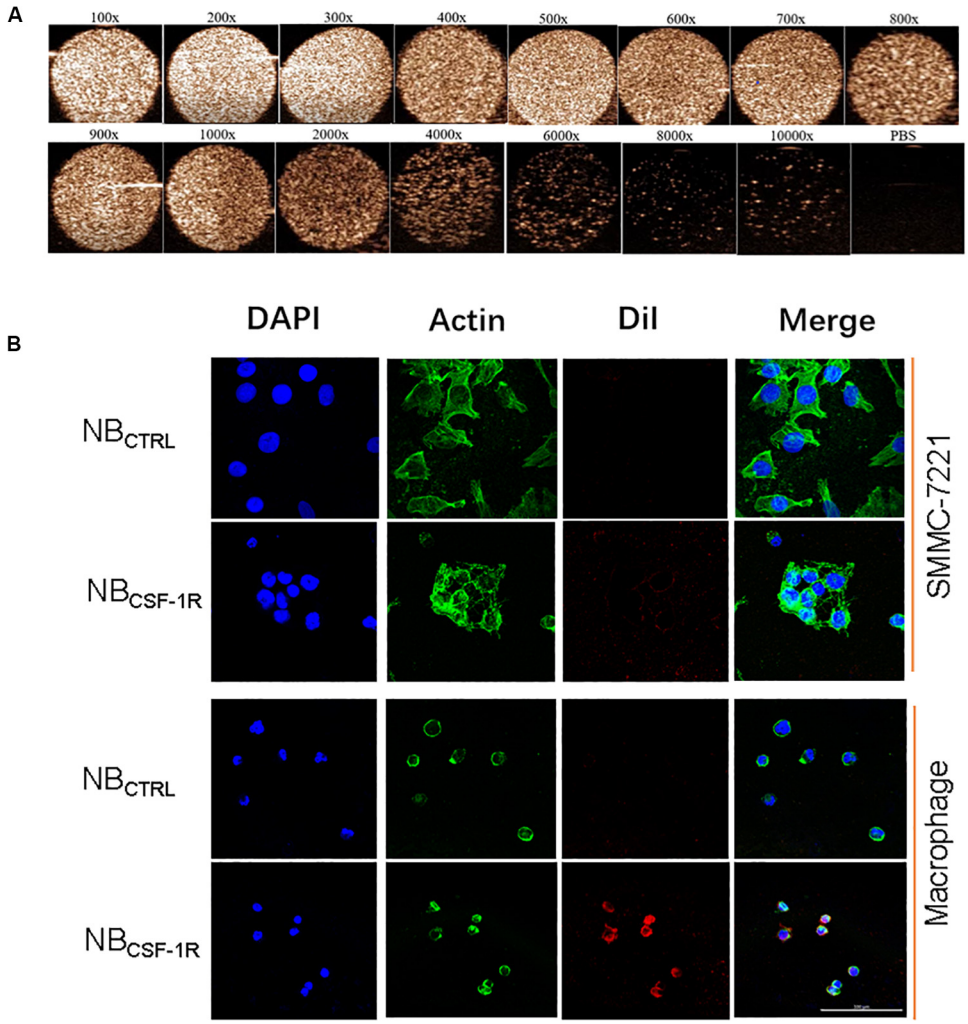


**FIGURE 6 | (A)** *In vitro* ultrasound images of various concentrations of $NB_{CSF-1R}$ dilute for different times, imaging was still viable even when diluted 2000 times. Ultrasound frequency, 20 MHz. **(B)** *In vitro*, the same quantity of $NB_{CSF-1R}$ and $NB_{CTRL}$ were added to SMMC-7721 and macrophages and then observed using confocal laser scanning microscopy (CLSM). There were few $NB_{CTRL}$ adhered to SMMC-7721 and macrophages, and also few $NB_{CTRL}$ bounded to macrophages. There were a lot $NB_{CSF-1R}$ bounded to macrophages, and showed the specificity of targeting. With a scale bar of 100 μm.

and 26.84 ± 0.44 min, 6.71 ± 0.07 min, 2.89 ± 0.44 min in IRFA models (**Figure 7D**). Therefore, in the xenograft tumors and IRFA models, the washout half-time (**Figure 7D**, $p = 0.05$) was significantly different between $NB_{CSF-1R}$, $NB_{CTRL}$, and Sonovue®. As shown in **Figures 7A,B**, even after 30 min, the $NB_{CSF-1R}$ contrast agent can still enhanced efficiently in xenograft tumors and IRFA models, which implied that it has a longer circulation time *in vivo*.

In the xenograft tumors, the echo signal intensity of $NB_{CSF-1R}$, $NB_{CTRL}$, and Sonovue® in the peritumoral tissues and tumor center are shown (**Figure 8**). The results indicated that the intensity of the peritumoral echo signal of $NB_{CSF-1R}$ was significantly higher than that of the central tissue (**Figures 8A,B**, $p = 0.05$) at the peak time, 5, and 15 min.

## Immunofluorescence Analysis of the Deposition of CSF-1

Colony-stimulating factor 1 receptor deposits were detected at the boundary of the tumor (**Figure 9A**), and were also detected at boundaries of the residual tumor after IRFA (**Figure 9C**). However, there were few deposits detected at the center of the tumor tissue (**Figure 9B**) or the residual tumor tissue (**Figure 9D**). The fluorescence intensity at the peritumor was higher than the tumor center. Therefore, similar to the human HCC spatial infiltration profiles, CSF-1R expressed in murine HCC were also abundant at the outer margins of the tumors. These results support the potential of using CSF-1R as a cancer imaging biomarker of macrophages.

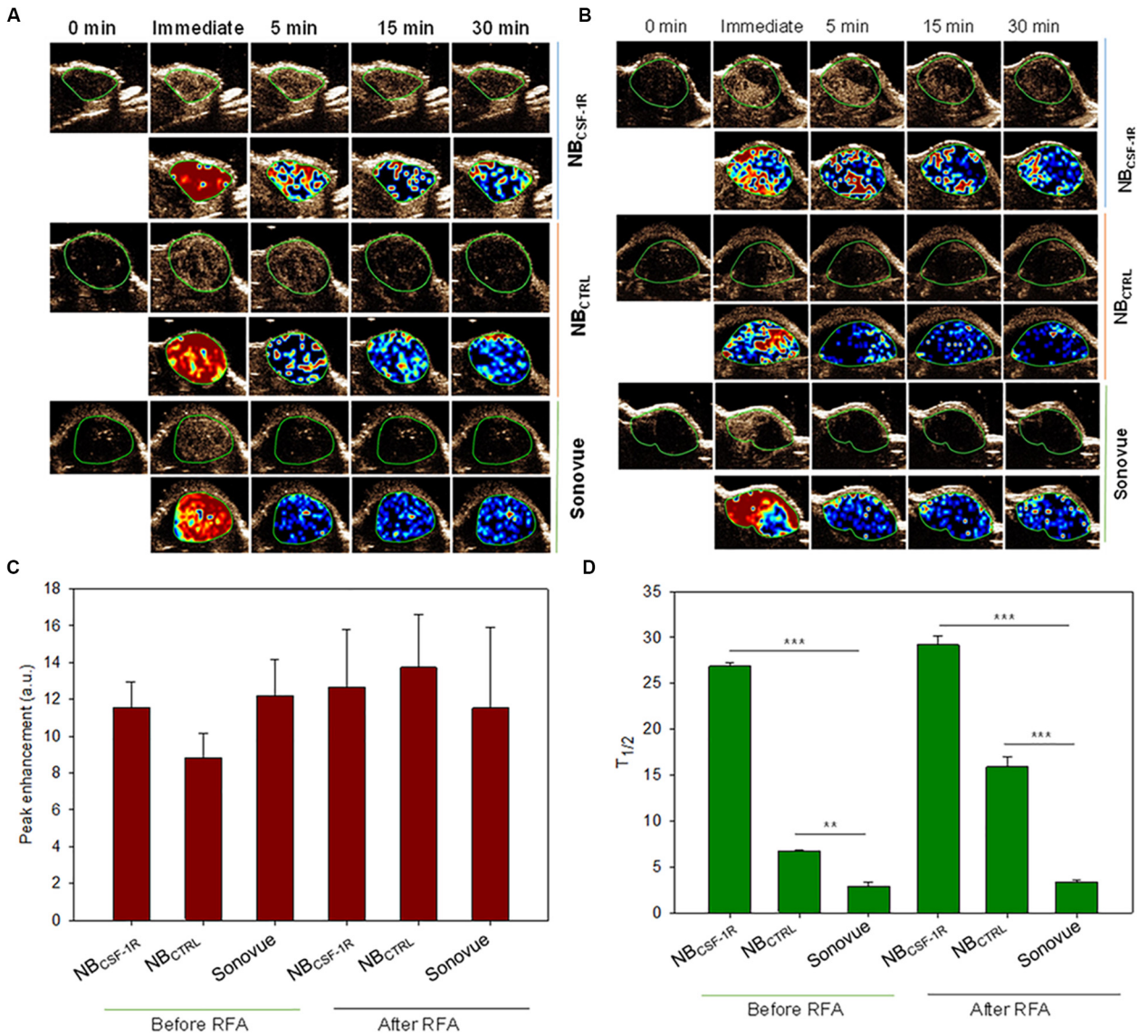


**FIGURE 7 | (A)** *In vivo* tumor imaging, images were taken at the indicated time points (0, immediate, 5, 15, and 30 min) after $NB_{CSF-1R}$, $NB_{CTRL}$, and Sonovue® were injected into tail vein of the transplanted tumors. **(B)** *In vivo* tumor imaging, images were taken at the indicated time points (0, immediate, 5, 15, and 30 min) after $NB_{CSF-1R}$, $NB_{CTRL}$, and Sonovue® were injected into tail vein of insufficient radiofrequency ablation (IRFA) models. Perfusion imaging was also taken to show the nanobubble diffusion. **(C)** The peak intensity of $NB_{CS-F1R}$, $NB_{CTRL}$, and Sonovue® was showed and there was no significant difference in each group. **(D)** The washout half-time in six group was show, and the $NB_{CSF-1R}$ can provide longer imaging time in the xenograft tumor and IRFA models (**indicates $p < 0.05$, ***indicates $p < 0.001$).

## DISCUSSION

Researches have shown that RFA can lead to acute serologic elevation of active cytokines such as IL-6, nMDSC, and mMDSC, and a sustained high infiltration level of macrophages in the residual tumor (Shi et al., 2019; Sugimoto et al., 2019). In this study, CSF-1R was found highly expressed at the tumor boundary in patients with HCC, and also highly expressed in macrophages, but not tumor cells; making CSF-1R a feasible target. Frozen sections of the tumors revealed that macrophages were mostly located at the boundary of the xenograft tumors and residual tissue after performing IRFA.

Nanobubble CSF-1R had an average size of about 428 nm and were ultrasound-visible even at 20 MHz both *in vitro* and *in vivo*; imaging was still viable even when diluted 2000 times. Notably, NBs were administered at a low concentration compared with our previous research and other studies (Wischhusen et al., 2018), a technique which can be employed to reduce the level of background signal and modulate facilitate the comparison of heterogeneous tumor models (Wang et al., 2010, 2016).

A

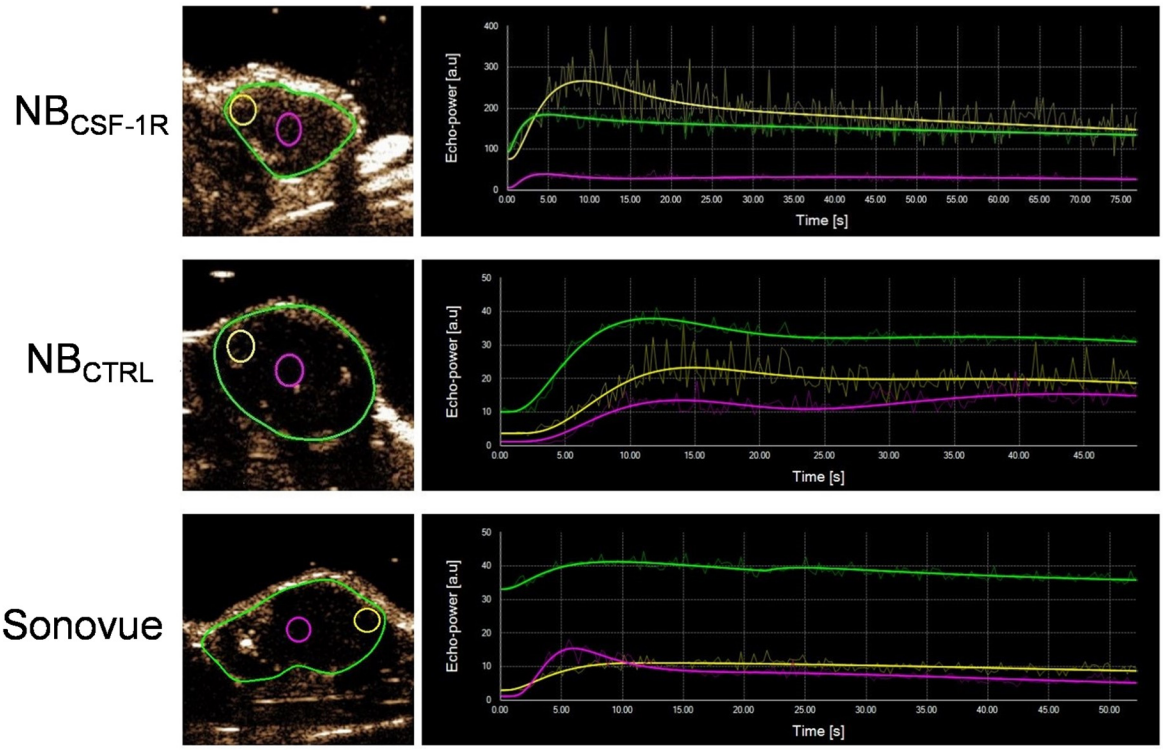


B

**Test statistics**

| | $TC_{pe}$ - $TP_{pe}$ | $TC_{5min}$ – $TP_{5min}$ | $TC_{15min}$ – $TP_{15min}$ | $NTC_{pe}$ – $NTP_{pe}$ | $BC_{5min}$ – $BP_{5min}$ | $BC_{15min}$ – $BP_{15min}$ | $SonoC_{pe}$ - $SonoP_{pe}$ |
|---|---|---|---|---|---|---|---|
| Z | -2.203[b] | -2.203[b] | -2.203[b] | -1.753[b] | -1.483[b] | -1.483[c] | -0.674[b] |
| P | 0.043 | 0.043 | 0.043 | 0.080 | 0.138 | 0.138 | 0.500 |

Wilcoxon signed-rank test; b = based on rank; c = based on negative rank
C = tumor center; P = peritumor; T = (Targeted) $NB_{CSF-1R}$, B = (Blank) $NB_{CTRL}$

**FIGURE 8 | (A)** The echo intensity fitting curve of the same area around or in the center of transplant tumor with $NB_{CSF-1R}$, $NB_{CTRL}$, and Sonovue®. The intensity of the peritumoral echo signal of the $NB_{CSF-1R}$ was significantly higher than that of the central tissue at the peak time, 5 and 15 min ($p = 0.05$). Data was shown in panel **(B)**.

To gain the insight functions of $NB_{CSF-1R}$, we explored the specificity and efficiency of targeting of NBs in SMMC-7721 cells and macrophages. The results confirmed that the CSF-1R antibody could bound onto NBs efficiently; and the resulting $NB_{CSF-1R}$ were stable and target specific. In an *in vitro* cell binding experiment, these $NB_{CSF-1R}$ were identified to aggregate selectively surrounding macrophages but not SMMC-7721 cells, implying that the attachment of NBs to CSF-1R-positive macrophages contributes to interactions between antigen and antibody. Moreover, unconjugated NBs did not bind to macrophages, suggesting that the CSF-1R antibodies conjugating on the surface of the NBs were able to specifically recognize and improve adhesion to macrophages with high CSF-1R expression. *In vivo*, non-invasive imaging modality can be applied in extra-vascular region once NBs penetrate deep into the tumor neovasculature with a feature of a maximum pore size of approximately 380—780; this is because a basement membrane and smooth muscle absent and the intercellular space expands in cancer vasculature (Maeda, 2015).

Reduction in the size of the MBs not only decreases its echogenicity under clinical ultrasound but also cause instability (Sheeran et al., 2013). In our *in vivo* imaging experiments,

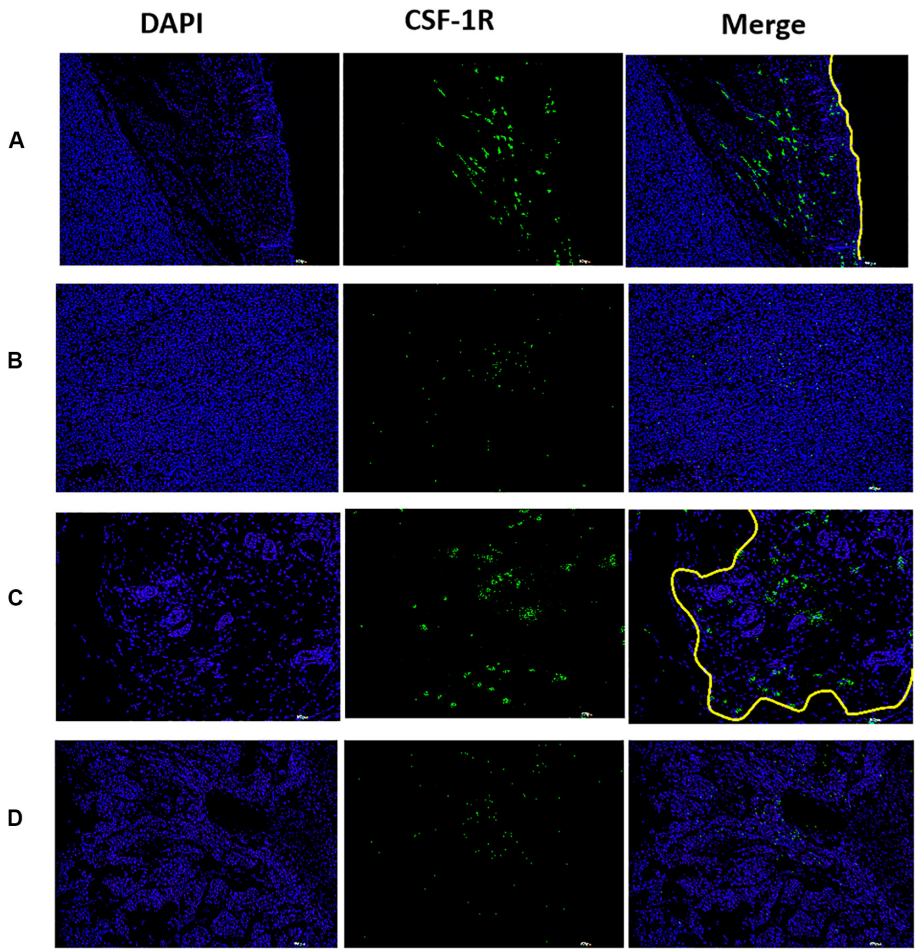


**FIGURE 9 |** The distribution of CSF-1R in xenograft tumor observed by fluorescence immunoassay, higher fluorescence intensity was observed at the peritumor, lower fluorescence intensity was observed at the tumor center. [**(A)** boundary of the tumor, **(B)** central of tumor, **(C)** boundary of the residual tumor after IRFA, and **(D)** residual tumor after IRFA. With a scale bar of 200 μm. The yellow line showed the tumor margin].

however, showed that the peak intensity of $NB_{CSF-1R}$, $NB_{CTRL}$, and Sonovue® had no statistical difference in the xenograft tumor models and IRFA models (**Figure 7C**). This is probably due to the fact that lipid contrast agents can produce preferable harmonic signal intensity (Postema and Schmitz, 2007), and nanoparticles could be accumulate within tumor tissue through the enhanced permeability and retention (EPR) effect and then were transformed into micro-sized echogenic bubbles (Min et al., 2016). These microbubbles at targeted tumor tissues could serve as new echogenic particles for cancer-targeting ultrasound imaging.

With the application of acoustic radiation forces (ARF) to upregulate contrast agent binding (Zhao et al., 2004), molecular ultrasound imaging is constantly improving. Frinking et al. (2012) manifested enhanced adhesion of targeted MB *in vivo* upon ARF performed in experimental models of cancer. In comparison with normal vessels, they found an increased binding of VEGFR2-targeted MB (BR55) in the vasculature of experiment (Frinking et al., 2012). In this study, in the xenograft tumor model and IRFA model, the washout half-time ratio of $NB_{CSF-1R}$ to NBs was two times higher, and about nine times higher compared to Sonovue®. Furthermore, being a nanoparticle, $NB_{CTRL}$ and $NB_{CSF-1R}$ could accumulate at the targeted tumor tissue via the EPR effect, and $NB_{CSF-1R}$ can abound onto higher CSF-1 expression cells effectively. The adherent $NB_{CSF-1R}$ maintained visible for a long time, contributing to a longer persistence of enhanced contrast compared to $NB_{CTRL}$ and Sonovue®. This result further verifies that the duration of contrast enhancement may be applied as an indicator for the investigation of targeted NBs enhanced imaging. The molecular imaging would also be helpful in finding the residual tumor after IRFA. With long-term stability, $NB_{CSF-1R}$ could be used to evaluate the boundary of the tumor when performing RFA.

## CONCLUSION

In this study, a uniform nano-sized lipid NBs was prepared, and could successfully combined the NBs with biotinylated

anti-CSF-1R. The $NB_{CSF-1R}$ which was small and stable as well as high specificity for the molecule that is overexpressed in macrophages. We demonstrated the high specificity of our $NB_{CSF-1R}$ on targeting CSF-1R overexpressing macrophages and HCC tumor margin. *In vitro* and *in vivo* studies demonstrated that $NB_{CSF-1R}$ exhibited effective ultrasound imaging capabilities in evaluating the RFA response, which can be used to detect the residual HCC after RFA, opening a possibility of clinical translation of a non-invasive diagnosis method for IRFA.

## DATA AVAILABILITY STATEMENT

All datasets generated for this study are included in the article/supplementary material.

## ETHICS STATEMENT

The animal study was reviewed and approved by Ethics Committee of Sun Yat-sen Memorial Hospital and Ethics Committee of Zhongshan School of Medicine (ZSSOM) on Laboratory Animal Care, Sun Yat-sen University.

## AUTHOR CONTRIBUTIONS

HL and BZ performed animal imaging analysis. YK performed statistical analysis. PS and BL designed and oversaw all the experiments and wrote the manuscript. All authors contributed to the article and approved the submitted version.

## FUNDING

This study was supported by the National Natural Science Foundation of China (81701715, 81671704, and 81873899); the Science Foundation of Guangdong Province (2017A030310200, 2016A030313306, 2017A030313727, and 2018A030313097); and the People's Livelihood and Technology Planning Project of Guangzhou City of China (201803010035).

## ACKNOWLEDGMENTS

We thank all the researchers and staff of the Guangdong Provincial Key Laboratory of Malignant Tumor Epigenetics and Gene Regulation for their contribution to this study, especially the flow cytometric analysis laboratory.

## REFERENCES

Chen, W., Zheng, R., Baade, P. D., Zhang, S., Zeng, H., Bray, F., et al. (2016). Cancer statistics in China, 2015. *CA Cancer J. Clin.* 66, 115–132. doi: 10.3322/caac.21338

Dai, H., Jia, G., Wang, H., Yang, J., Jiang, H., and Chu, M. (2017). Epidermal growth factor receptor transactivation is involved in the induction of human hepatoma SMMC7721 cell proliferation by insufficient radiofrequency ablation. *Oncol. Lett.* 14, 2463–2467. doi: 10.3892/ol.2017.6463

Frinking, P. J., Tardy, I., Theraulaz, M., Arditi, M., Powers, J., Pochon, S., et al. (2012). Effects of acoustic radiation force on the binding efficiency of BR55, a VEGFR2-specific ultrasound contrast agent. *Ultrasound Med. Biol.* 38, 1460–1469. doi: 10.1016/j.ultrasmedbio.2012.03.018

Guvener, N., Appold, L., de Lorenzi, F., Golombek, S. K., Rizzo, L. Y., Lammers, T., et al. (2017). Recent advances in ultrasound-based diagnosis and therapy with micro- and nanometer-sized formulations. *Methods* 130, 4–13. doi: 10.1016/j.ymeth.2017.05.018

Jia, J. B., Wang, W. Q., Sun, H. C., Zhu, X. D., Liu, L., and Zhuang, P. Y. (2010). High expression of macrophage colony-stimulating factor-1 receptor in peritumoral liver tissue is associated with poor outcome in hepatocellular carcinoma after curative resection. *Oncologist* 15, 732–743. doi: 10.1634/theoncologist.2009-0170

Jiang, Q., Hao, S., Xiao, X., Yao, J., Ou, B., Zhao, Z., et al. (2016). Production and characterization of a novel long-acting Herceptin-targeted nanobubble contrast agent specific for Her-2-positive breast cancers. *Breast Cancer Tokyo* 23, 445–455. doi: 10.1007/s12282-014-0581-8

Kang, T. W., Kim, J. M., Rhim, H., Lee, M. W., Kim, Y. S., and Lim, H. K. (2015). Small hepatocellular carcinoma: radiofrequency ablation versus nonanatomic resection–propensity score analyses of long-term outcomes. *Radiology* 275, 908–919. doi: 10.1148/radiol.15141483

Kim, Y. S., Lee, W. J., Rhim, H., Lim, H. K., Choi, D., and Lee, J. Y. (2010). The minimal ablative margin of radiofrequency ablation of hepatocellular carcinoma (>2 and <5 cm) needed to prevent local tumor progression: 3D quantitative assessment using CT image fusion. *AJR Am. J. Roentgenol.* 195, 758–765. doi: 10.2214/AJR.09.2954

Kong, L. Q., Zhu, X. D., Xu, H. X., Zhang, J. B., Lu, L., and Wang, W. Q. (2013). The clinical significance of the CD163+ and CD68+ macrophages in patients with hepatocellular carcinoma. *PLoS One* 8:e59771. doi: 10.1371/journal.pone.0059771

Krupka, T. M., Solorio, L., Wilson, R. E., Wu, H., Azar, N., and Exner, A. A. (2010). Formulation and characterization of echogenic lipid-Pluronic nanobubbles. *Mol. Pharm.* 7, 49–59. doi: 10.1021/mp9001816

Leftin, A., Ben-Chetrit, N., Joyce, J. A., and Koutcher, J. A. (2019). Imaging endogenous macrophage iron deposits reveals a metabolic biomarker of polarized tumor macrophage infiltration and response to CSF1R breast cancer immunotherapy. *Sci. Rep.* 9:857. doi: 10.1038/s41598-018-37408-7

Lewis, C. E., and Pollard, J. W. (2006). Distinct role of macrophages in different tumor microenvironments. *Cancer Res.* 66, 605–612. doi: 10.1158/0008-5472.CAN-05-4005

Li, X., Wang, D., Ran, H., Hao, L., Cao, Y., Ao, M., et al. (2018). A preliminary study of photoacoustic/ultrasound dual-mode imaging in melanoma using MAGE-targeted gold nanoparticles. *Biochem. Biophys. Res. Commun.* 502, 255–261. doi: 10.1016/j.bbrc.2018.05.155

Liu, R., Tang, J., Xu, Y., and Dai, Z. (2019). bioluminescence imaging of inflammation in vivo based on bioluminescence and fluorescence resonance energy transfer using nanobubble ultrasound contrast agent. *ACS Nano* 13, 5124–5132. doi: 10.1021/acsnano.8b08359

Liu, Z., Dai, H., Jia, G., Li, Y., Liu, X., and Ren, W. (2015). Insufficient radiofrequency ablation promotes human hepatoma SMMC7721 cell proliferation by stimulating vascular endothelial growth factor overexpression. *Oncol. Lett.* 9, 1893–1896. doi: 10.3892/ol.2015.2966

Maeda, H. (2015). Toward a full understanding of the EPR effect in primary and metastatic tumors as well as issues related to its heterogeneity. *Adv. Drug Deliv. Rev.* 91, 3–6. doi: 10.1016/j.addr.2015.01.002

Min, H. S., Son, S., You, D. G., Lee, T. W., Lee, J., Lee, S., et al. (2016). Chemical gas-generating nanoparticles for tumor-targeted ultrasound imaging and ultrasound-triggered drug delivery. *Biomaterials* 108, 57–70. doi: 10.1016/j.biomaterials.2016.08.049

Muralidhara, S., Malu, K., Gaines, P., and Budhlall, B. M. (2019). Quantum dot encapsulated nanocolloidal bioconjugates function as bioprobes for in vitro intracellular imaging. *Colloids Surf. B Biointerfaces* 182, 110348. doi: 10.1016/j.colsurfb.2019.110348

Nandi, S., Cioce, M., Yeung, Y. G., Nieves, E., Tesfa, L., and Lin, H. (2013). Receptor-type protein-tyrosine phosphatase zeta is a functional receptor for interleukin-34. *J. Biol. Chem.* 288, 21972–21986. doi: 10.1074/jbc.M112.442731

N'Kontchou, G., Mahamoudi, A., Aout, M., Ganne-Carrie, N., Grando, V., and Coderc, E. (2009). Radiofrequency ablation of hepatocellular carcinoma: long-term results and prognostic factors in 235 Western patients with cirrhosis. *Hepatology* 50, 1475–1483. doi: 10.1002/hep.23181

Postema, M., and Schmitz, G. (2007). Ultrasonic bubbles in medicine: influence of the shell. *Ultrason. Sonochem.* 14, 438–444. doi: 10.1016/j.ultsonch.2006.09.013

Pyonteck, S. M., Akkari, L., Schuhmacher, A. J., Bowman, R. L., Sevenich, L., Quail, D. F., et al. (2013). CSF-1R inhibition alters macrophage polarization and blocks glioma progression. *Nat. Med.* 19, 1264–1272. doi: 10.1038/nm.3337

Qian, B. Z., and Pollard, J. W. (2010). Macrophage diversity enhances tumor progression and metastasis. *Cell* 141, 39–51. doi: 10.1016/j.cell.2010.03.014

Shady, W., Petre, E. N., Gonen, M., Erinjeri, J. P., Brown, K. T., Covey, A. M., et al. (2016). Percutaneous radiofrequency ablation of colorectal cancer liver metastases: factors affecting outcomes–A 10-year experience at a single center. *Radiology* 278, 601–611. doi: 10.1148/radiol.2015142489

Sheeran, P. S., Streeter, J. E., Mullin, L. B., Matsunaga, T. O., and Dayton, P. A. (2013). Toward ultrasound molecular imaging with phase-change contrast agents: an in vitro proof of principle. *Ultrasound Med. Biol* 39, 893–902. doi: 10.1016/j.ultrasmedbio.2012.11.017

Shi, L., Wang, J., Ding, N., Zhang, Y., and Liao, W. (2019). Inflammation induced by incomplete radiofrequency ablation accelerates tumor progression and hinders PD-1 immunotherapy. *Nat. Commun.* 10:5421.

Sotirchos, V. S., Petrovic, L. M., Gonen, M., Klimstra, D. S., Do, R. K., and Petre, E. N. (2016). Colorectal cancer liver metastases: biopsy of the ablation zone and margins can be used to predict oncologic outcome. *Radiology* 280, 949–959. doi: 10.1148/radiol.2016151005

Sugimoto, K., Kakimi, K., Takeuchi, H., Fujieda, N., and Itoi, T. (2019). Irreversible electroporation versus radiofrequency ablation: comparison of systemic immune responses in patients with hepatocellular carcinoma. *J. Vasc. Int. Radiol.* 30, 845.e6–853.e6.

Tang, H., Zheng, Y., and Chen, Y. (2017). Materials chemistry of nanoultrasonic biomedicine. *Adv. Mater.* 29:1604105. doi: 10.1002/adma.201604105

Wang, L., Chen, S., Zhu, Y., Zhang, M., Tang, S., Li, J., et al. (2018). Triple-modal imaging-guided chemo-photothermal synergistic therapy for breast cancer with magnetically targeted phase-shifted nanoparticles. *ACS Appl. Mater. Interfaces* 10, 42102–42114. doi: 10.1021/acsami.8b16323

Wang, P., Wang, X., Luo, Q., Li, Y., Lin, X., Fan, L., et al. (2019). Fabrication of red blood cell-based multimodal theranostic probes for second near-infrared window fluorescence imaging-guided tumor surgery and photodynamic therapy. *Theranostics* 9, 369–380. doi: 10.7150/thno.29817

Wang, S., Herbst, E. B., Mauldin, F. J., Diakova, G. B., Klibanov, A. L., and Hossack, J. A. (2016). Ultra-low-dose ultrasound molecular imaging for the detection of angiogenesis in a mouse murine tumor model: how little can we see? *Invest. Radiol.* 51, 758–766. doi: 10.1097/RLI.0000000000000310

Wang, X., Sofocleous, C. T., Erinjeri, J. P., Petre, E. N., Gonen, M., and Do, K. G. (2013). Margin size is an independent predictor of local tumor progression after ablation of colon cancer liver metastases. *Cardiovasc. Intervent. Radiol.* 36, 166–175. doi: 10.1007/s00270-012-0377-1

Wang, Y., Li, X., Zhou, Y., Huang, P., and Xu, Y. (2010). Preparation of nanobubbles for ultrasound imaging and intracelluar drug delivery. *Int. J. Pharm.* 384, 148–153. doi: 10.1016/j.ijpharm.2009.09.027

Wischhusen, J., Wilson, K. E., Delcros, J. G., Molina-Pena, R., Gibert, B., Jiang, S., et al. (2018). Ultrasound molecular imaging as a non-invasive companion diagnostic for netrin-1 interference therapy in breast cancer. *Theranostics* 8, 5126–5142. doi: 10.7150/thno.27221

Zhang, N., Li, H., Qin, C., Ma, D., Zhao, Y., Zhu, W., et al. (2019). Insufficient radiofrequency ablation promotes the metastasis of residual hepatocellular carcinoma cells via upregulating flotillin proteins. *J. Cancer Res. Clin. Oncol.* 145, 895–907. doi: 10.1007/s00432-019-02852-z

Zhao, S., Borden, M., Bloch, S. H., Kruse, D., Ferrara, K. W., and Dayton, P. A. (2004). Radiation-force assisted targeting facilitates ultrasonic molecular imaging. *Mol. Imaging* 3, 135–148. doi: 10.1162/15353500423 80317

Zhou, B., Jiang, Q., Xiao, X., Xu, X., Xu, Y., Kong, Y., et al. (2019). Assisting anti-PD-1 antibody treatment with a liposomal system capable of recruiting immune cells. *Nanoscale* 11, 7996–8011. doi: 10.1039/c9nr01434a

Zhu, X. D., Zhang, J. B., Zhuang, P. Y., Zhu, H. G., Zhang, W., and Xiong, Y. Q. (2008). High expression of macrophage colony-stimulating factor in peritumoral liver tissue is associated with poor survival after curative resection of hepatocellular carcinoma. *J. Clin. Oncol.* 26, 2707–2716. doi: 10.1200/JCO. 2007.15.6521

**Conflict of Interest:** The authors declare that the research was conducted in the absence of any commercial or financial relationships that could be construed as a potential conflict of interest.